Water Science & Technology

IWA PUBLISHING

Water Science & Technology Vol 84 No 5, 1090 doi: 10.2166/wst.2021.296

Synergistically homogeneous-heterogeneous Fenton catalysis of trace copper ion and g-C_3N_4 for degradation of organic pollutants

Z. Y. Yao, G. X. Zhu, T. L. Lu and Y. Z. Zhan*

School of Chemical Engineering, Zhengzhou University, Zhengzhou 450001, China
*Corresponding author. E-mail: zhanyz@zzu.edu.cn

TLL, 0000-0003-3000-2122; YZZ, 0000-0002-3817-6373

ABSTRACT

Using the bulk g-C_3N_4 as a precursor, four g-C_3N_4 nanosheets were further prepared by ultrasonic, thermal, acid, and alkali exfoliation. The structures of these materials were characterized by various techniques such as X-ray powder diffraction, Fourier transform infrared spectroscopy, scanning electron microscopy, energy dispersive X-ray spectroscopy, transmission electron microscopy, and X-ray photoelectron spectroscopy. The synergistical Fenton catalysis of these materials with Cu^{2+} was evaluated by using rhodamine B as a simulated organic pollutant. The results showed that there existed a significant synergistical Fenton catalysis between Cu^{2+} and g-C_3N_4. This synergistic effect can be observed even when the concentration of Cu^{2+} was as low as 0.064 mg L^{-1}. The properties of g-C_3N_4 strongly influenced the catalytic activity of the Cu^{2+}/g-C_3N_4 system. The coexistent of Cu^{2+} and the alkali exfoliated g-C_3N_4 showed the best catalytic activity. Hydroxyl radicals as oxidizing species were confirmed in the Cu^{2+}/g-C_3N_4 system by electron paramagnetic resonance spectra. The synergistic catalysis may be attributed to the easier reduction of Cu^{2+} adsorbed on the g-C_3N_4. This study provided an excellent Fenton catalytic system, and partly solved the rapid deactivation of heterogeneous Fenton catalysts caused by the leaching of metal ions.

Key words: advanced oxidation process, copper, heterogeneous Fenton catalyst, synergistical catalysis, g-C_3N_4

HIGHLIGHTS

- There exists a significant synergistical Fenton catalysis between trace Cu^{2+} and g-C_3N_4.
- The Cu^{2+} concentration is lower than the maximum acceptable limit in drinking water.
- This study partly solved the rapid deactivation caused by the leaching of metal ions.
- This study reminds researchers to pay attention to the possible synergistic catalysis between leached ions and supports.

GRAPHICAL ABSTRACT

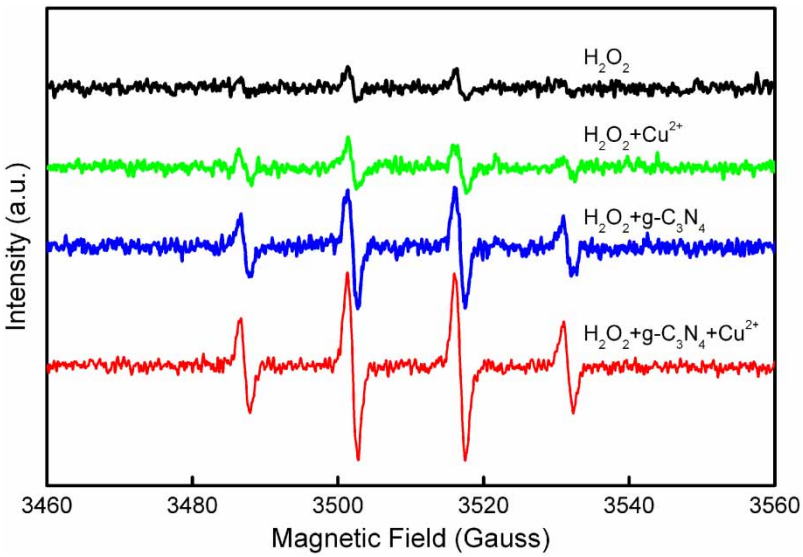

INTRODUCTION

Direct discharging of wastewaters containing refractory organics, such as dyes, phenols, drugs, and insecticides, seriously threatens the safety of environment. Economically treating these wastewaters is still a difficult task. Among various treating strategies based on physical, chemical, and biological principles, advanced oxidation processes (AOPs) are the most attractive techniques, because these processes generate strongly oxidizing radical species (primarily HO·) affording the potential for transforming the refractory pollutants to non-toxic small molecules like water, carbon dioxide, and inorganic salts. One of the AOPs, the classical homogeneous Fenton process, which activates H_2O_2 generating HO· through the redox cycle of Fe^{2+}/Fe^{3+}, has been extensively studied and commercially applied (Lin *et al.* 2020). However, some problems existing in this process increase the operating costs. For example, the pH should be controlled at about 3, thus the wastewater has to be acidified before treatment and neutralized before discharge. This process also produces large amounts of iron sludge, requiring further disposal. To overcome these difficulties, increasing attention has been paid to heterogeneous Fenton systems, i.e. using solid Fe-containing materials as catalysts to activate H_2O_2. In recent decades, many iron compounds and supported iron materials as heterogeneous Fenton catalysts have been studied (Zhu *et al.* 2019). In addition, other metals including Ag, Al, Ce, Co, Cr, Cu, Mn, and Ru as catalytically active species in heterogeneous Fenton systems have also received attention (Bokare & Choi 2014). Among these metals, copper is the most important non-iron active species studied both in homogeneous and heterogeneous Fenton systems, because copper shows higher catalytic activity than other metals over a wide pH range (Bokare & Choi 2014; Gu *et al.* 2019). The Cu(II)-catalyzed Fenton reaction was generally considered to be based on the redox cycle of Cu(I)/Cu(II) to activate H_2O_2, similar to the redox cycle of Fe^{2+}/Fe^{3+} (Nichela *et al.* 2013).

Leaching of metal ions is a fatal disadvantage of these solid catalysts (Zhu *et al.* 2019). This leaching not only leads to catalyst deactivation rapidly, but also raises the question whether the sites of the Fenton reaction are metal ions in the solid phase or the leached metal ions dissolved in the homogeneously aqueous phase. Obviously, it is vital work to identify the Fenton catalysis through homogeneous or heterogeneous mechanism (Kuan *et al.* 2015). Some studies showed that the Fenton catalysis was attributed to homogeneous mechanism of the leached metal ions from solid catalysts, some studies have suggested that the catalysis depended on the combination of homogeneous and heterogeneous mechanisms. However, most studies using solid catalysts simply assumed that the Fenton reaction proceeded through heterogeneous routes. Some studies have carried out experiments to ascertain the presence of heterogeneous mechanisms. The approaches employed included: (i) checking the catalytic activity of filtrates; (ii) adjusting solutions at alkaline/near-neutral pH to prevent metal ions leaching; (iii) comparing pollutant degradation kinetics in homogeneous and heterogeneous Fenton systems; and (iv) analyzing the concentration of leached metal ions. When the concentration of the metal ions was found to be small, the reaction was assumed to be through a heterogeneous route (Kuan *et al.* 2015).

Kuan *et al.* (2015) studied the Fenton oxidation of 4-chlorophenol in the presence of FeO_x/TiO_2 or $CuFe_2O_4$ as a catalyst. Using inductively coupled plasma-optical emission spectroscopy (ICP-OES) in combination with pH monitoring and ultraviolet-visible spectroscopy (UV-vis), they monitored the degradation of 4-chlorophenol over the two Fenton heterogeneous systems. The results showed that these two systems proceeded predominantly through a homogeneous route via dissolved metal ions from the solid catalysts, and sub-ppm levels of Fe and Cu ions dissolved from the solid phases were sufficient to explain the observed 4-chlorophenol degradation rates. They also pointed out that the above four approaches employed to ascertain the presence of heterogeneous catalytic routes cannot exclude the homogeneous Fenton route in the presence of solid catalysts.

Another problem ignored by researchers is the possible interaction between dissolved metal ions and solid catalyst supports. It has been reported that carbon materials as supports can significantly accelerate the reduction of Fe(III) to Fe(II), the rate-limiting step in the heterogeneous Fenton reaction, resulting in the enhancement of the decomposition of H_2O_2 and the production of HO· (Zhu *et al.* 2020a). Obviously, a reasonable guess can be proposed that the carbon supports may also adsorb the dissolved metal ions such as Fe^{3+} and Cu^{2+} and promote their reduction, thus enhancing the Fenton catalytic activities. That is to say, there may be synergistic catalysis between metal ions and carbon supports. This point, as far as we know, has not been reported. In fact, carbon material can be used not only as supports of heterogeneous Fenton catalysts, but also as heterogeneous Fenton catalysts (Navalon *et al.* 2011). Carbon materials as heterogeneous Fenton catalysts on their own have received increasing interest in recent years, because there is no problem of metal ion leaching in this kind of metal-free catalysts. Carbon materials studied as heterogeneous Fenton catalysts have included activated carbon, carbon black, biochar, carbon nanotube, carbon xerogel, glycerol-based carbon, carbon quantum dots, graphite, graphene, etc. Among these carbon materials, graphene, a well known 2D carbon material, has attracted the most intensive attention. Graphene, graphene oxide, and reduced graphene oxide have been all studied as heterogeneous metal-free catalysts for Fenton processes (Zhu *et al.* 2020b).

Graphitic carbon nitride (g-C_3N_4) is another well known 2D carbon material, which has a similar structure as graphene. g-C_3N_4 materials were mainly used as photocatalysts (Li *et al.* 2020), and also used as catalyst supports, including as heterogeneous Fenton catalyst supports (Ding *et al.* 2019; Wang & Nan 2020). Recently, we reported the performance of g-C_3N_4 as a heterogeneous Fenton catalyst for the first time (Zhu *et al.* 2020b). We found that even unmodified g-C_3N_4 prepared by the conventional urea pyrolysis was still an effective heterogeneous Fenton catalyst over a wide pH range. However, the catalytic activity of the g-C_3N_4 was not high at room temperature. In this study, we used rhodamine B as a simulated organic pollutant, and investigated the synergistically homogeneous–heterogeneous Fenton catalysis of trace Cu^{2+} and g-C_3N_4. The results showed that the Fenton catalytic activity in the presence of both Cu^{2+} and g-C_3N_4 was much higher than that in the presence of Cu^{2+} or g-C_3N_4 alone. When g-C_3N_4 nanosheets replaced the convenient bulk g-C_3N_4, excellent catalytic activity can be observed.

METHODS

Materials

Urea was purchased from Tianjin Fengchuan Chemical Reagent Co., Ltd (Tianjin, China). Methanol, absolute alcohol, $Cu(NO_3)_2{\cdot}3H_2O$, KOH, HCl (36%), H_2SO_4 (98%), NaOH, ethylenediamine tetraacetic acid (EDTA), rhodamine B (RhB), isopropanol, and H_2O_2 (30%) were purchased from Sinopharm Chemical Reagent Co., Ltd (Shanghai, China). These reagents were of analytical grade and were used without further purification.

Preparation of bulk g-C_3N_4

The bulk g-C_3N_4 was synthesized by conventional urea pyrolysis (Liu *et al.* 2011; Zhu *et al.* 2020b). Urea was dried at 80 °C for 1 h in a crucible with a cover. Then the crucible was heated to 580 °C with a heating rate of about 3 °C min^{-1} in a muffle furnace, and remained at 580 °C for 3 h. The product was washed successively with 0.1 mol L^{-1} HCl, deionized water, and absolute alcohol until the filtrate was neutral. Lastly, the wet sample was dried in a vacuum freeze dryer for 10 h.

Preparation of ultrasonic exfoliated g-C_3N_4

The bulk g-C_3N_4 of 0.1 g was dispersed in 100 mL methanol. The mixture was treated with ultrasound for 4 h using a JN-5200DT sonicator (Ningbo Jiangnan Instrument Factory, China) working at 40 kHz and 200 W. The product was separated by centrifugation, washed to neutrality, and dried at 105 °C (Zhao *et al.* 2014).

Preparation of thermal exfoliated g-C_3N_4

The nanosheet was prepared by thermal oxidation etching of the bulk g-C_3N_4 in air (Niu *et al.* 2012). The bulk g-C_3N_4 in a crucible was heated to 580 °C with a heating rate of 5 °C min^{-1} and kept at 580 °C for 2 h.

Preparation of acid exfoliated g-C_3N_4

The bulk g-C_3N_4 of 2 g was dispersed in 40 mL H_2SO_4 (98%). The mixture was stirred at room temperature for 8 h, and then slowly poured into 200 mL deionized water. The temperature of the mixture increased rapidly, and the color changed from yellow to light yellow. After ultrasound treatment for 4 h, the product was separated by centrifugation, washed to neutrality, and dried at 105 °C (Xu *et al.* 2013).

Preparation of alkali exfoliated g-C_3N_4

The colloidal g-C_3N_4 nanosheet was obtained by exfoliating the bulk g-C_3N_4 in KOH aqueous solution (Li *et al.* 2017). The bulk g-C_3N_4 of 0.5 g was dispersed in a 40 ml KOH aqueous solution of 5 mol L^{-1}. The mixture was stirred at 80 °C for 12 h. In this period the mixture gradually became a transparent colloid. After centrifuging the colloid to remove small amounts of residue residue, the re-stacked g-C_3N_4 was obtained by adding HCl solution to the transparent colloid. The product was washed with water and dried at 60 °C.

Characterization of g-C_3N_4

Powder X-ray diffraction (XRD) data were collected on a Bruker D8 Advance diffractometer with Cu Kα radiation. Fourier transform infrared (FTIR) spectra were obtained on a WQF-510 infrared spectrophotometer (Beijing Rayleigh Analytical Instrument Corp., China) using the KBr disc method. Scanning electron microscope (SEM) images were recorded on a JEOL JSM-7500F scanning electron microscope. Transmission electron microscopy (TEM) images were obtained using a Tecnai G2F20 S-Twin TMP electron microscope. X-ray photoelectron spectroscopy (XPS) measurements were conducted on a Thermo Scientific-Escalb 250XI electron spectrometer. The electron paramagnetic resonance (EPR) spectra were recorded on a Bruker EMX Plus EPR spectrometer. 5,5-Dimethyl-1-pyrroline *N*-oxide (DMPO) was used as a radical trapping agent.

Catalytic degradation of RhB

Typically, 100 mL RhB solution with a concentration of 50 mg/L was used as simulated wastewater to evaluate the catalytic performance of the studied systems. The degradation of RhB was carried out in a glass reactor of 250 mL immersed in a constant temperature water bath with magnetic stirring. The initial solution pH was adjusted using a small amount of 0.1 mol L^{-1} HCl or 0.1 mol L^{-1} NaOH solution. After adding the g-C_3N_4 and Cu^{2+} solution into the RhB solution, the mixture was stirred for 30 min to achieve adsorption–desorption equilibrium. Then the reaction was started by adding a certain amount of H_2O_2 solution. Unless otherwise specified, the reaction temperature was 25 °C, the initial pH was 9, the amount of g-C_3N_4 was 0.2 g L^{-1}, the concentration of Cu^{2+} was 0.64 mg L^{-1}, and the initial concentration of H_2O_2 was 50 mmol L^{-1}. At predetermined time intervals, a 4 mL reaction solution was taken out. After immediate centrifugation, the concentration of RhB was analyzed at 554 nm using an INESA 722G spectrophotometer. The decolorization efficiency of the dye was calculated based on the residual concentration. The UV-vis absorption spectra of the reaction solution were recorded by using a Shimadzu UV-2600 spectrophotometer.

To study the effect of variables on the degradation, the experiments were repeated under different initial pH values, g-C_3N_4 dosages, Cu^{2+} concentrations, H_2O_2 concentrations, dye concentrations and temperatures. As a comparison, Cu^{2+} could be replaced by Ni^{2+}, Zn^{2+}, Fe^{2+}, or Fe^{3+}. EDTA or Fe(III)-EDTA can also be added to the reaction system to study their effects. The degradation of various other dyes was also carried out under typical conditions. The free radical capture experiment was carried out under typical conditions, but adding isopropanol into the degradation solution to 60 mmol L^{-1}.

RESULTS AND DISCUSSION

Characterization of bulk g-C_3N_4 and g-C_3N_4 nanosheets

The XRD patterns of the prepared bulk g-C_3N_4 and g-C_3N_4 nanosheets are shown in Figure 1. The crystal structure of the bulk g-C_3N_4 was verified by its XRD data (Liu *et al.* 2011). The sharp peak at 27.5° was indicative of the graphitic stacking structure, which was indexed as (002). The calculated stacking distance of aromatic units is 0.324 nm. A weak peak at 12.8° was attributed to the in-planar repeating unit, which was indexed as (100). Compared with the bulk g-C_3N_4, the XRD pattern of the sample prepared by ultrasonic exfoliation almost did not change, indicating that this g-C_3N_4 sample still remained as a

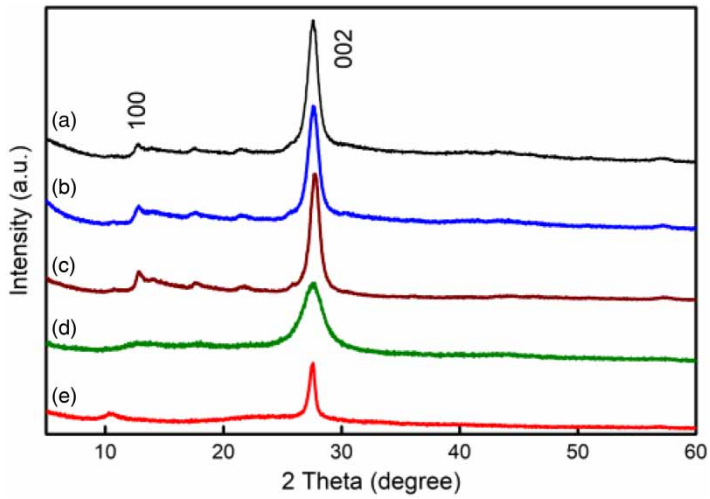

Figure 1 | XRD patterns of (a) bulk g-C_3N_4 and g-C_3N_4 nanosheets prepared via (b) ultrasonic, (c) thermal, (d) acid, and (e) alkali exfoliation.

larger size after the ultrasound treatment. For the sample prepared by thermal exfoliation, the sharp peak slight shifted from 27.5° to 27.7°, and the calculated stacking distance of aromatic units decreased to 0.322 nm, indicating that the thermal treatment resulted in a more condensed packing of g-C_3N_4 (Niu *et al.* 2012). After acid exfoliation, the XRD peak at 27.5° obviously decreased and widened, and the peak at 12.8° almost disappeared, showing the formation of nano-sized ultrathin nanosheets (Xu *et al.* 2013).

The alkali treatment of the bulk g-C_3N_4 resulted in a transparent colloid. This was significantly different from the above bulk and exfoliated g-C_3N_4 as these particles were visible to the naked eye. The sample after alkali exfoliation used to be characterized came from restacking of the dissolved g-C_3N_4 nanosheet by adding HCl. From its XRD pattern it was found that this re-stacked material still presented the typical structural features of g-C_3N_4. However, the peak at 27.5° obviously decreased, and the peak at 12.8° substantially shifted to10.3°, indicating that this material had a larger 'hole to hole' distance compared with the other g-C_3N_4 samples (Li *et al.* 2017).

The structures of the prepared bulk g-C_3N_4 and g-C_3N_4 nanosheets were further characterized by FTIR (Figure 2). The results indicated that all the prepared exfoliated samples preserved the main structure of the bulk g-C_3N_4 (Liu *et al.* 2011; Sudhaik *et al.* 2018). The wide band between 3,000 and 3,500 cm^{-1} was attributed to an uncondensed amino N–H stretching vibration. The strong bands at 1,630, 1,569, 1,454, and 1,395 cm^{-1} were assigned to the stretching vibration of

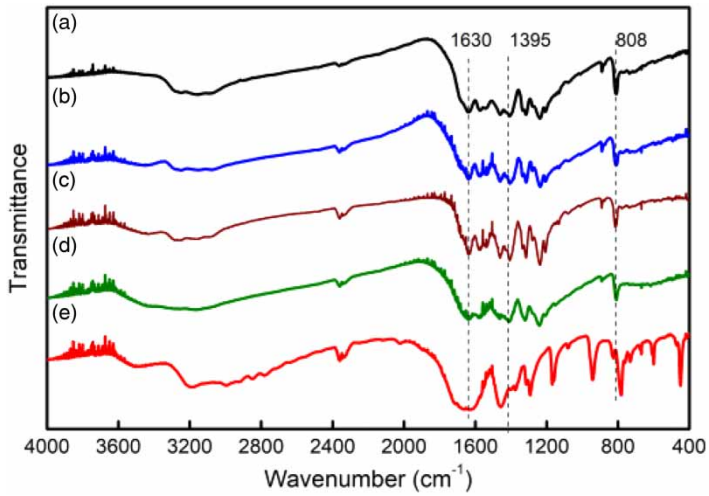

Figure 2 | FTIR spectra of (a) bulk g-C_3N_4 and g-C_3N_4 nanosheets prepared via (b) ultrasonic, (c) thermal, (d) acid, and (e) alkali exfoliation.

heptazine-derived repeating units. The bands at 1,313 and 1,229 cm^{-1} corresponded to the stretching vibration of connected units of $N–(C)_3$ or C–NH–C. The sharp band at 808 cm^{-1} represented the out-of-plane bending vibration of heptazine rings. However, there were some additional bands appearing in the alkali exfoliated sample. These bands could be attributed to the oxygen-containing groups generated from the alkali treatment of g-C_3N_4. The band at about 3,400 cm^{-1} could be assigned to the absorbed or substituted OH groups. The shoulder band at about 1,700 cm^{-1} indicated the formation of the C = O group. The bands at 451, 600, 732, 782, 829, 944, and 1,163 cm^{-1} may be related to the bending vibration of oxygen-containing groups. In addition, the band at 808 cm^{-1}, which represented the out-of-plane bending vibration of heptazine rings, shifted slightly to 782 cm^{-1}.

The morphology of the g-C_3N_4 samples is shown in Figure 3. The as-prepared bulk g-C_3N_4 showed loose aggregation of thin sheets. Its specific surface area was measured as about 77 $m^2\,g^{-1}$, near the values for g-C_3N_4 prepared by using similar methods (Liu *et al.* 2011; Sudhaik *et al.* 2018). All of the four exfoliated g-C_3N_4 samples generally showed the stacking structure of nanosheets, although their morphologies were different. In addition, the thin chiffon-like nanosheets could be observed from the TEM image of the re-stacked sample of the alkali exfoliated g-C_3N_4.

In view of the fact that the alkali exfoliated g-C_3N_4 exhibited the best catalytic performance among the prepared g-C_3N_4 samples (see below), the XPS technique was employed to further detect any changes in the surface groups. As shown in Figure 4, the survey scan showed that the bulk g-C_3N_4 was composed primarily of carbon and nitrogen. The very weak O1s peak commonly observed in XPS spectra of g-C_3N_4 may come from adsorbed oxygen. However, in the survey scan of the alkali exfoliated g-C_3N_4, the C1s and N1s peaks decreased significantly, meanwhile, an obvious enhanced O1s peak could be observed, indicating that the treatment of alkali exfoliation resulted in partial destruction of the g-C_3N_4 structure and formation of oxygen-containing groups. The high-resolution spectrum of O1s showed that the deconvoluted three peaks at 531.8, 532.7, and 533.8 eV, were attributed to oxygen of O = C, O–C and O–H, respectively. Accordingly, two new C1s peaks at 286.1 eV and 289.0 eV, attributed to carbon of O–C and O = C–O, respectively, can be deconvoluted from the C1s high-resolution spectrum of the alkali exfoliated g-C_3N_4 (Pisanu *et al.* 2018). In addition, the deconvoluted peak corresponded to sp2-bonded carbon (N–C = N) decreased significantly and shifted slightly from 288.0 eV to 288.6 eV. The weak peak at 284.8 eV, which was attributed to graphitic carbon and usually appeared on the XPS characterization for g-C_3N_4, also decreased. The high-resolution spectrum of N1 s showed that the deconvoluted three peaks at 398.6, 400.2, and 401.3 eV, which could be attributed to sp2 hybrid nitrogen (C–N=C), tertiary nitrogen ($N–(C)_3$), and amino groups with a hydrogen atom (C–N–H), respectively, still existed after treatment with alkali exfoliation. The peak deconvoluted at 399.6 eV was attributed to the new N-containing group resulting from the alkali treatment.

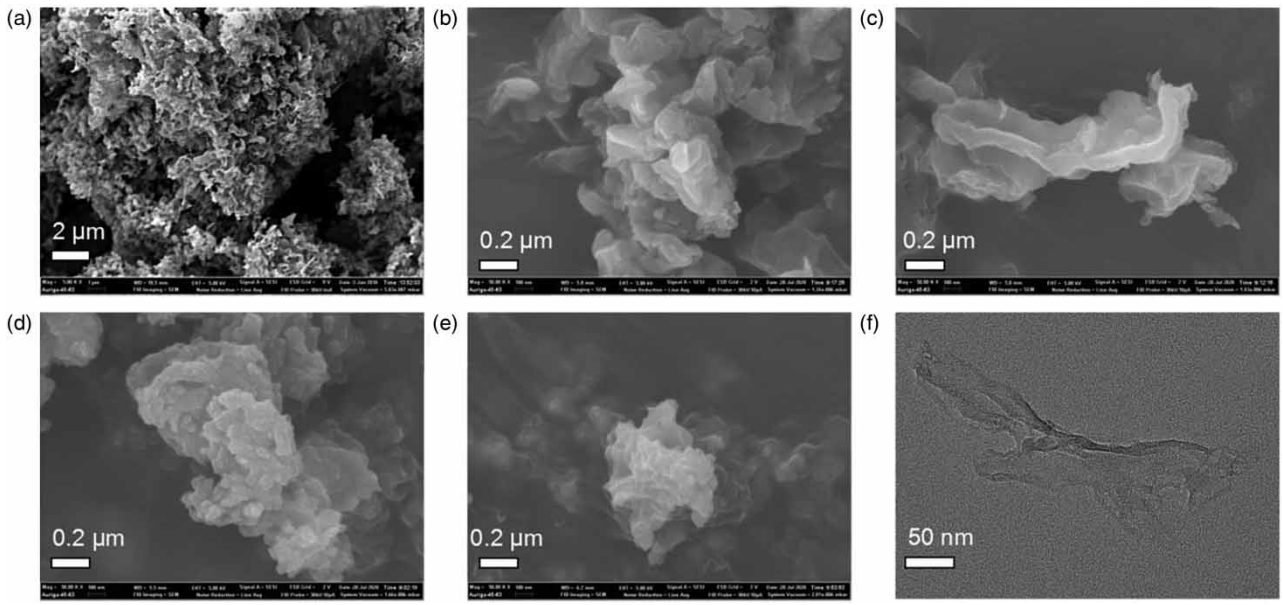

Figure 3 | SEM images of (a) bulk g-C_3N_4 and g-C_3N_4 nanosheets prepared via (b) ultrasonic, (c) thermal, (d) acid, and (e) alkali exfoliation. (f) TEM image of alkali exfoliated g-C_3N_4.

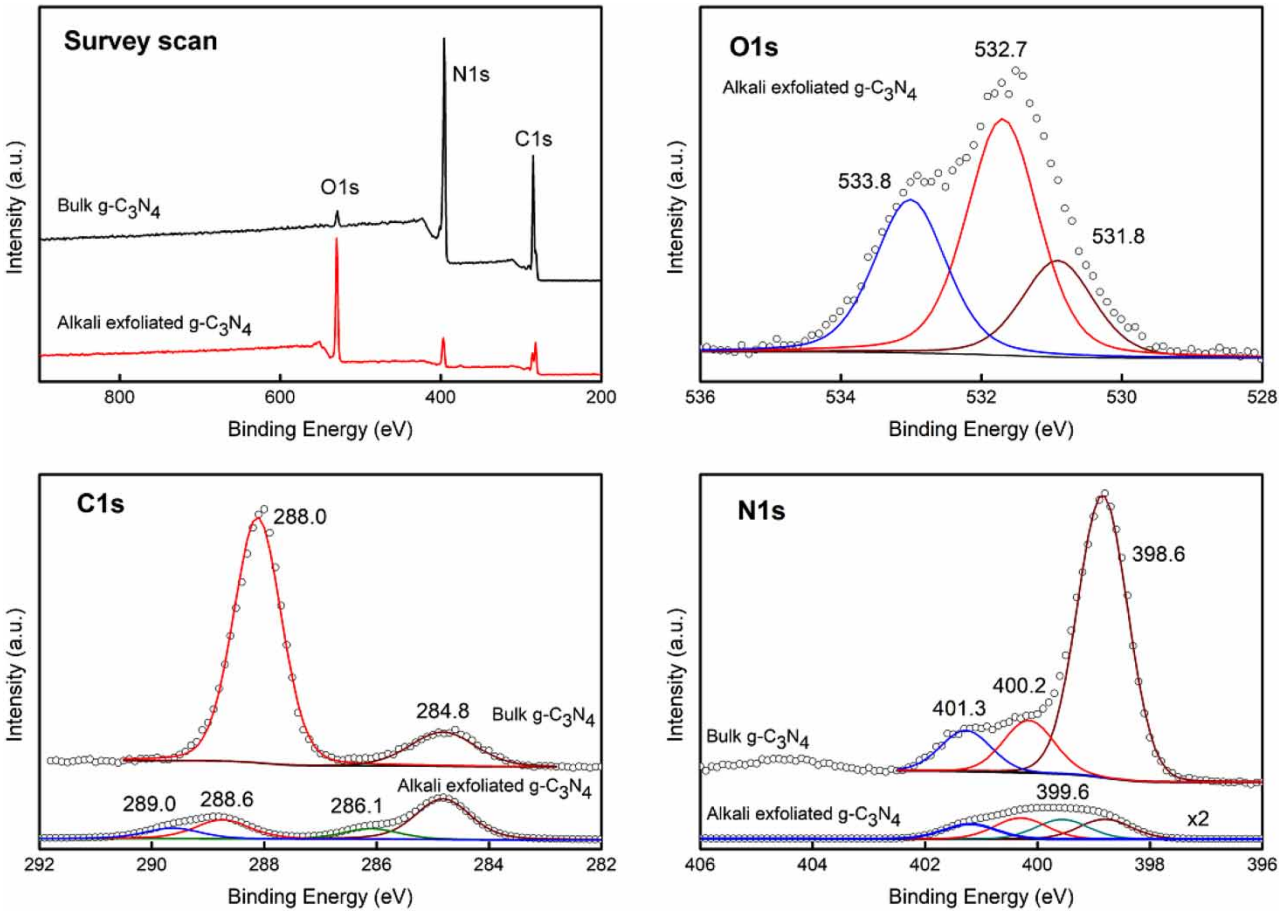

Figure 4 | Comparison of XPS survey spectra, O1s, C1s, and N1s of bulk g-C_3N_4 and alkali exfoliated g-C_3N_4.

Synergistic catalysis between Cu^{2+} and bulk g-C_3N_4

The existence of synergistic catalysis between Cu^{2+} and g-C_3N_4 was firstly proved by using the bulk g-C_3N_4 (Figure 5). At pH 5 and 50 °C, the bulk g-C_3N_4 alone showed only weak catalytic activity, and the decolorization efficiency was only about 20% in 140 min, and the catalytic activity of Cu^{2+} with the concentration as low at 0.064 mg L^{-1} was nearly same as that of the bulk g-C_3N_4. However, when the two coexisted, the catalytic activity was obviously improved. In this case the decolorization efficiency was more than 60% in 140 min, clearly showing the synergistic catalysis between the two.

Further increasing the concentration of Cu^{2+} to 0.64 mg L^{-1}, the catalytic activity of Cu^{2+} was obviously improved, and the dye degradation efficiency reached about 60% in 140 minutes. However, when this Cu^{2+} coexisted with the bulk g-C_3N_4, the decolorization efficiency reached more than 90% in the same period, showing excellent catalytic performance. Moreover, this Cu^{2+} concentration was even lower than the maximum acceptable limit of Cu^{2+} concentration in drinking water. The discharge of wastewater containing Cu^{2+} with this concentration should not cause environmental pollution. The higher concentration of Cu^{2+} would conceal the synergistic effect because of its obvious catalytic activity (Figure S1, Supporting information). Moreover, the discharge of Cu^{2+} with high concentrations will cause environmental pollution.

The synergistic catalysis at different pH was investigated by using the bulk g-C_3N_4 (Figure 6). The results showed that there was synergistic catalysis in the range of pH 3–9. In particular, at pH 5 the synergistic effect was most obvious. Under alkaline conditions, the catalytic activity of single Cu^{2+} was higher than that of the bulk g-C_3N_4, partially concealing the synergistic effect.

It should be pointed out that, although the above investigation doubtlessly proved that there was a synergistic effect between Cu^{2+} and the bulk g-C_3N_4, higher catalytic activity emerged only at higher temperatures. At room temperature the catalytic activity was relatively low. For example, at 50 °C, the degradation efficiency reached more than 90% in 140 min, while at

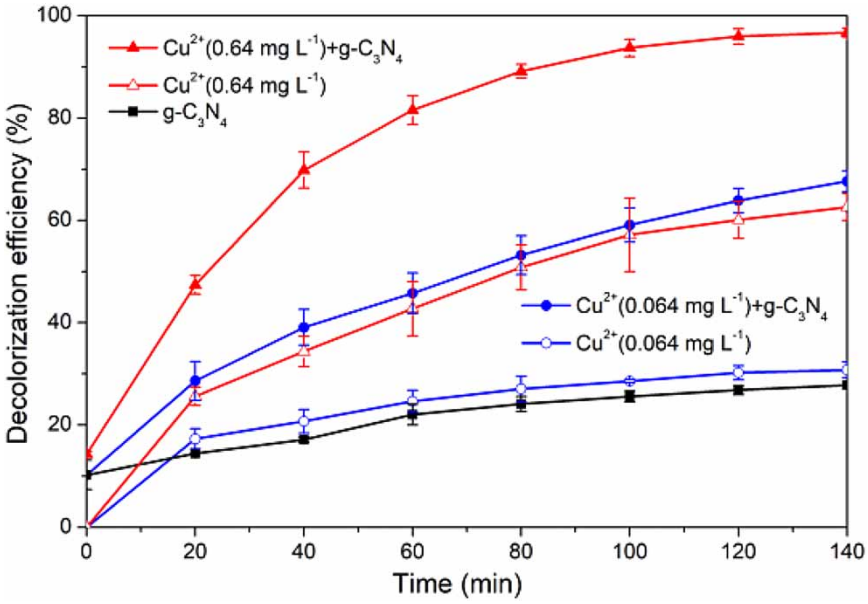

Figure 5 | Effect of copper ion concentration on synergetic catalysis. The slight decolorization at Time = 0 was caused by the adsorption of the bulk g-C_3N_4.

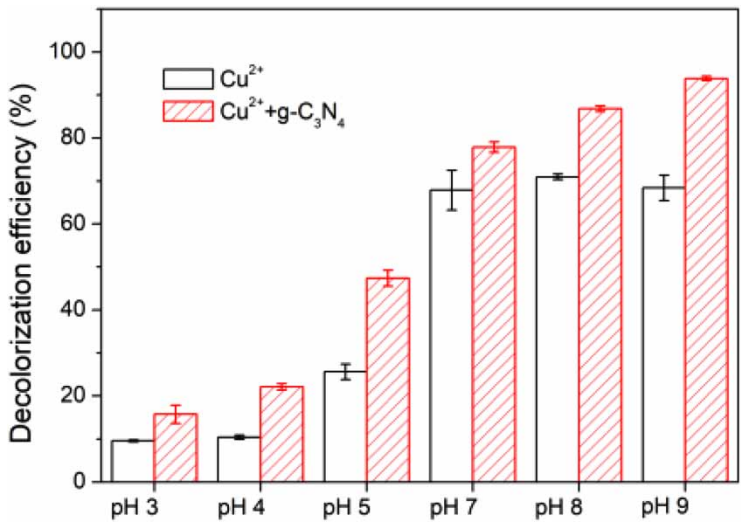

Figure 6 | Effect of pH on synergetic catalysis (20 min).

30 °C, it was only about 40% (Figure S2). This may be due to the lack of active sites provided by the bulk g-C_3N_4. Therefore, we prepared four g-C_3N_4 nanosheets via various exfoliations and studied their synergistic catalysis with Cu^{2+} to expectantly obtain high catalytic activity at room temperature.

Synergistic catalysis between Cu^{2+} and g-C_3N_4 nanosheets

Figure 7 and Figure S3 show the catalytic activities of the g-C_3N_4 samples with and without Cu^{2+} at pH 9 and 25 °C. In the absence of Cu^{2+}, the Fenton catalytic activity of the g-C_3N_4 nanosheets prepared by different methods was obviously higher than that of the bulk g-C_3N_4. When each nanosheet separately coexisted with Cu^{2+}, the synergistic catalysis was more significant than that of the Cu^{2+} and bulk g-C_3N_4 system. In particular, the alkali applied g-C_3N_4 and Cu^{2+} system exhibited the best catalytic performance. The dye degradation efficiency reached about 97% in 10 min at room temperature, which was much

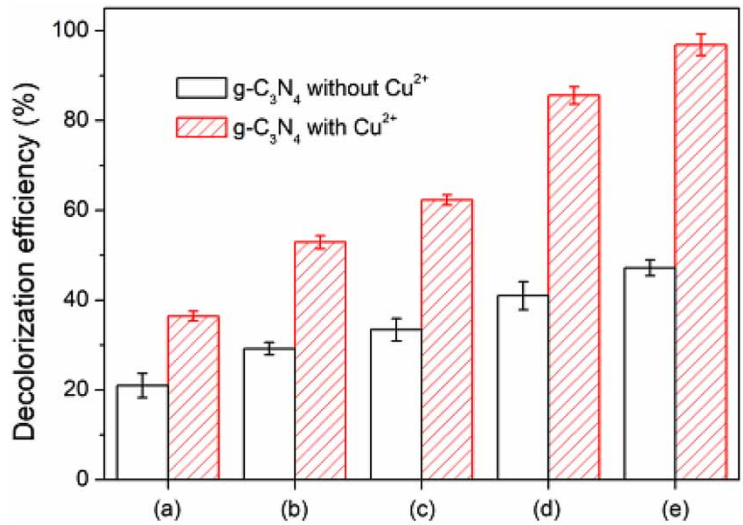

Figure 7 | Effect of (a) bulk g-C_3N_4 and g-C_3N_4 nanosheet prepared via (b) ultrasonic, (c) thermal, (d) acid, and (e) alkali exfoliation on synergetic catalysis (10 min).

better than that of the Cu^{2+} and bulk g-C_3N_4 system. Even if the concentration of Cu^{2+} was reduced to 0.064 mg L^{-1}, the mixed system still showed fairly good catalytic activity. The degradation efficiency of the dye reached 75% in 10 min and 90% in 60 min (Figure 8).

The effect of pH value on the catalytic performance of the alkali exfoliated g-C_3N_4 and Cu^{2+} system was also investigated (Figure 9). It was found that the catalytic activity was excellent in the range pH 7–9. The activity decreased when the pH dropped below 6. In fact, the re-stacked product of the alkali exfoliated g-C_3N_4 could dissolve in water under alkaline condition, forming a transparent solution. This may be one of the reasons for its high activity. When the pH value decreased, the system was turbid, indicating the precipitation of g-C_3N_4 via restacking.

The alkali exfoliated g-C_3N_4 and trace Cu^{2+} constituted an excellent synergistic catalytic system. This system still showed high degradation efficiency for RhB under the condition of low g-C_3N_4 dosage (0.05 g L^{-1}), low concentration of H_2O_2 (5 mmol L^{-1}), and higher dye concentration (100 mg L^{-1}). It also performed well in degradation of various other dyes (Figure S4). Compared with recently reported catalysts for heterogeneous Fenton degradation of RhB, this synergistic system displayed quite excellent catalytic activity, as shown in Table S1 (Supporting information).

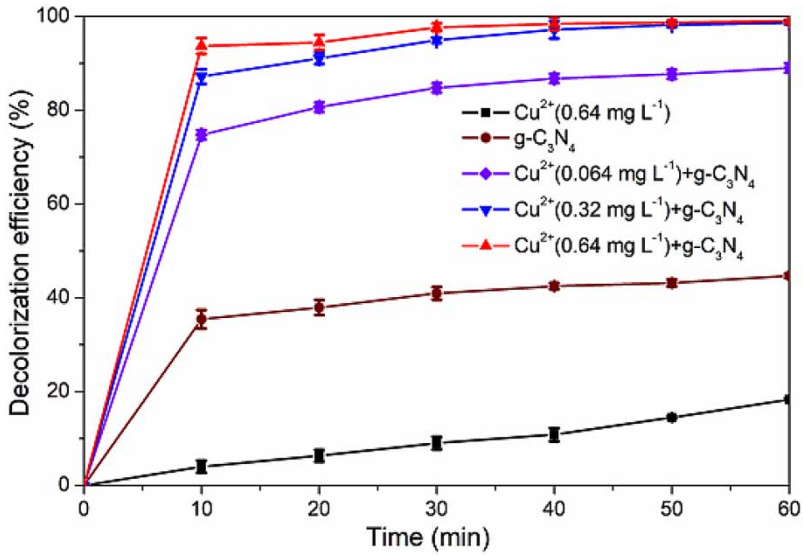

Figure 8 | Effect of copper ion concentration on synergetic catalysis.

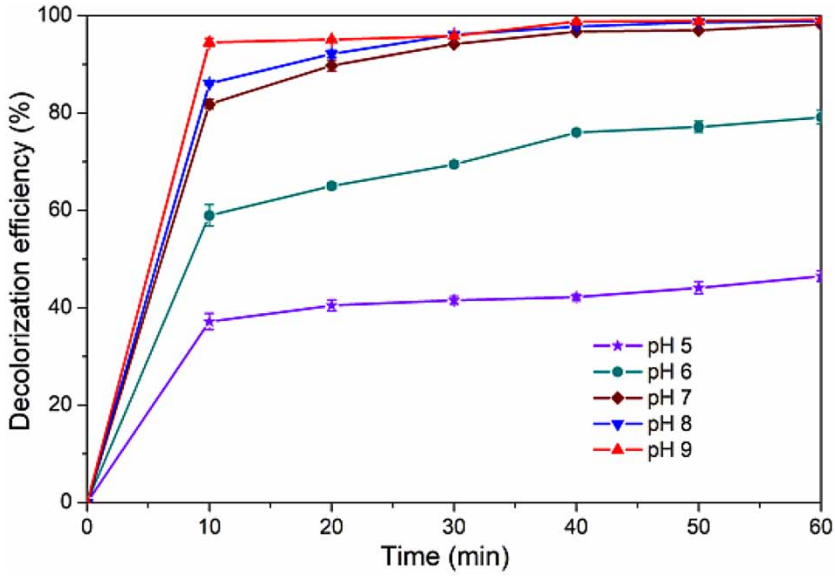

Figure 9 | Effect of pH on synergetic catalysis.

Possible mechanism

Hydroxyl radicals (HO·) generated by activating H_2O_2 as oxidizing species were confirmed in the Cu^{2+}/g-C_3N_4 system by the characteristic electron spin resonance (ESR) spectrum of DMPO-OH spin adduct (Figure 10). As controlled experiments, a very weak signal can be observed in the presence of H_2O_2 alone without Cu^{2+} and g-C_3N_4, it may be due to the decomposition of H_2O_2 caused by impurities. In the presence of Cu^{2+}, the signal was slightly enhanced, indicating that the low concentration Cu^{2+} had only a weak ability to activate H_2O_2. In the presence of the alkali exfoliated g-C_3N_4, the signal became stronger, indicating that the alkali exfoliated g-C_3N_4 had obvious Fenton catalytic activity. However, in the presence of Cu^{2+} and the alkali exfoliated g-C_3N_4, the signal significantly enhanced, clearly indicating that the Cu^{2+} and the alkali exfoliated g-C_3N_4 had a synergistic Fenton catalytic effect. From the UV-vis spectra of the reaction solution in Figure S5, it can be found that the structure of the xanthene-conjugated chromophore (554 nm) of the RhB molecule was destroyed quickly by hydroxyl radicals.

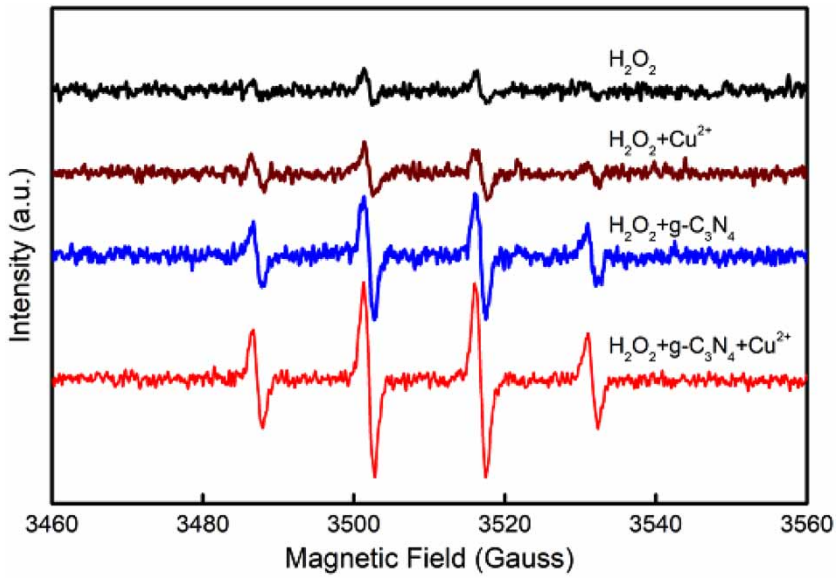

Figure 10 | EPR spectra of DMPO-OH in various systems.

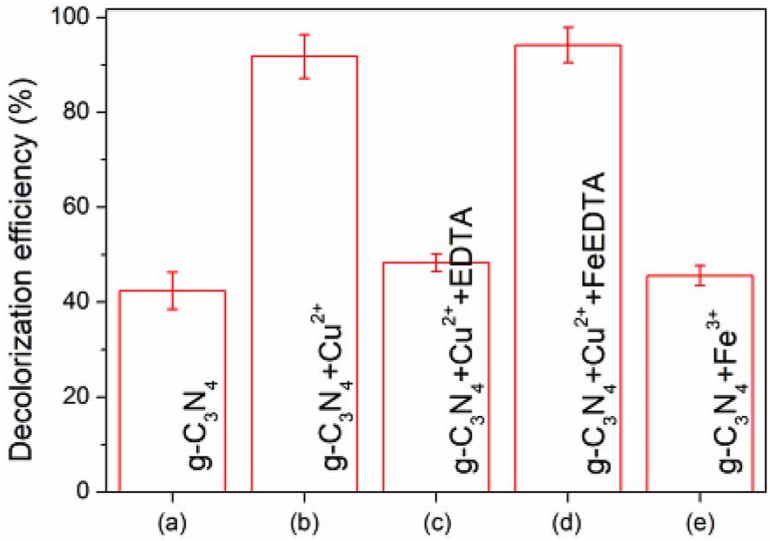

Figure 11 | Effect of adding EDTA on synergetic catalysis.

That HO· was the major reactive oxidizing species was further supported by a scavenging experiment of free radicals. The addition of isopropanol, a HO· scavenger, in the Cu^{2+} and the alkali exfoliated g-C_3N_4 system significantly decreased the degradation of RhB (Figure S6).

As mentioned above, homogeneous Cu^{2+} as a Fenton catalyst has been extensively studied. It is generally believed that the activation of H_2O_2 to generate HO· is through a Cu^{2+}/Cu^{+} redox cycle mechanism, similar to the Fe^{3+}/Fe^{2+} cycle. However, if the Cu^{2+} concentration is as low as less than 1 mg L^{-1}, its catalytic activity is difficult to detect. For the Cu^{2+} and g-C_3N_4 system we can reasonably speculate that Cu^{2+}, which is adsorbed on the g-C_3N_4, was the active sites of the Fenton catalysis. Mainly in these sites H_2O_2 was activated to generate HO·. The catalysis of the unabsorbed homogeneous Cu^{2+} in the aqueous phase can be ignored due to its very low concentration. The catalysis of the g-C_3N_4 itself may only contribute slightly to the dye degradation. For other ions with the same concentration, such as Ni^{2+}, Zn^{2+}, even Fe^{2+}, the classical Fenton catalyst, did not enhance the catalytic activity of the bulk g-C_3N_4. Adding these ions to the Cu^{2+} and bulk g-C_3N_4 system also did not influence the catalytic activity (Figure S7).

It should be pointed out that the adsorbed Cu^{2+} is different from the supported Cu^{2+}. The existence of adsorbed Cu^{2+} depends on the dissolved Cu^{2+} in the solution. To examine this idea, we carried out several preliminary experiments. We measured the aqueous equilibrium concentration of Cu^{2+} in the Cu^{2+} and bulk g-C_3N_4 system and found that it was obviously lower than its initial concentration. The bulk g-C_3N_4 was separated from the equilibrium system, washed with water, and dried, then used to catalytically degrade the dye without adding additional Cu^{2+}. It was found that this g-C_3N_4 performed obviously higher activity than the original g-C_3N_4, but lower activity than the Cu^{2+} and bulk g-C_3N_4 systems (Figure S8). This implied that there existed absorbed Cu^{2+} on the separated g-C_3N_4. We also added EDTA into the Cu^{2+} and alkali exfoliated g-C_3N_4 system and found that the synergistical effect of Cu^{2+} completely disappeared due to the formation of stable Cu-EDTA complexes. However, when adding more stable Fe-EDTA complexes in the system, the catalytic activity was not influenced as in this case EDTA did not react with Cu^{2+}. As a control, the replacement of Cu^{2+} by Fe^{3+} with the same concentration did not accelerate the Fenton catalytic activity of the g-C_3N_4 (Figure 11).

Previous results have shown that the properties of g-C_3N_4 strongly affected the catalytic activity of the Cu^{2+}/g-C_3N_4 system. The role of g-C_3N_4 may not only be used as adsorbent to enrich Cu^{2+}. Its conductivity and surface groups may contribute to the reduction of Cu^{2+}, which is the rate controlling step of the Fenton reaction. These problems need to be further studied.

CONCLUSIONS

There may exist synergistic catalysis between the metal ions leached from heterogeneous Fenton catalysts and the supports. This problem seems to have been ignored in previous relevant research. This study, may be for the first time, confirmed that a significant synergistical Fenton catalysis between trace Cu^{2+} and g-C_3N_4 exists. The properties of g-C_3N_4 strongly influenced

the catalytic activity of the Cu^{2+}/g-C_3N_4 system. The coexistence of Cu^{2+} and the alkali exfoliated g-C_3N_4 showed the best catalytic activity. Synergistic catalysis may be attributed to the easier reduction of Cu^{2+} adsorbed onto g-C_3N_4. The discharge of Cu^{2+} with concentrations below 1 mg L^{-1} would not threaten the safety of the water environment. This study partly solved the rapid deactivation of heterogeneous Fenton catalysts caused by leaching of metal ions, and also reminds researchers to pay attention to the possible synergistic catalysis between leached Cu^{2+} and carbon supports when using copper supported on carbon materials as heterogeneous Fenton catalysts. The recovery of g-C_3N_4 nanosheets is still a problem. An obvious strategy is to combine g-C_3N_4 with magnetic materials, thus the catalyst could be recovered by magnetic separation. In addition, as the discussion of the mechanism in this study is still at an early stage, further in-depth exploration is necessary.

ACKNOWLEDGEMENTS

We are grateful to the National Natural Science Foundation of China (21802125) and the Henan Science and Technology Project (172102210490) for financial support.

CONFLICT OF INTEREST

There are no conflicts to declare.

DATA AVAILABILITY STATEMENT

All relevant data are included in the paper or its Supplementary Information.

REFERENCES

Bokare, A. D. & Choi, W. 2014 Review of iron-free Fenton-like systems for activating H_2O_2 in advanced oxidation processes. *Journal of Hazardous Materials* **275**, 121–135. https://doi.org/10.1016/j.jhazmat.2014.04.054.

Ding, Q., Lam, F. L. & Hu, X. 2019 Complete degradation of ciprofloxacin over g-C_3N_4-iron oxide composite via heterogeneous dark Fenton reaction. *Journal of Environmental Management* **244**, 23–32. doi:10.1016/j.jenvman.2019.05.035.

Gu, T., Dong, H. X., Lu, T. L., Han, L. & Zhan, Y. Z. 2019 Fluoride ion accelerating degradation of organic pollutants by Cu(II)-catalyzed Fenton-like reaction at wide pH range. *Journal of Hazardous Materials* **377**, 365–370. https://doi.org/10.1016/j.jhazmat.2019.05.073.

Kuan, C. C., Chang, S. Y. & Schroeder, S. L. M. 2015 Fenton-like oxidation of 4-chlorophenol: homogeneous or heterogeneous? *Industrial & Engineering Chemistry Research* **54**, 8122–8129. https://doi.org/10.1021/acs.iecr.5b02378.

Li, G., Li, L., Yuan, H., Wang, H., Zeng, H. & Shi, J. 2017 Alkali-assisted mild aqueous exfoliation for single-layered and structure-preserved graphitic carbon nitride nanosheets. *Journal of Colloid and Interface Science* **495**, 19–26. https://doi.org/10.1016/j.jcis.2017.01.112.

Li, Y., Li, X., Zhang, H. W., Fan, J. J. & Xiang, Q. J. 2020 Design and application of active sites in g-C_3N_4-based photocatalysts. *Journal of Materials Science & Technology* **56**, 69–88. https://doi.org/10.1016/j.jmst.2020.03.033.

Lin, X. Q., Kong, W. M. & Lin, X. 2020 Degradation of high-concentration p-nitrophenol by Fenton oxidation. *Water Science and Technology* **81**, 2260–2269. https://doi.org/10.2166/wst.2020.284.

Liu, J., Zhang, T., Wang, Z., Dawson, G. & Chen, W. 2011 Simple pyrolysis of urea into graphitic carbon nitride with recyclable adsorption and photocatalytic activity. *Journal of Materials Chemistry* **21**, 14398–14401. https://doi.org/10.1039/C1JM12620B.

Navalon, S., Dhakshinamoorthy, A., Alvaro, M. & Garcia, H. 2011 Heterogeneous Fenton catalysts based on activated carbon and related materials. *Chemsuschem* **4**, 1712–1730. https://doi.org/10.1002/cssc.201100216.

Nichela, D. A., Berkovic, A. M., Costante, M. R., Juliarena, M. P. & García Einschlag, F. S. 2013 Nitrobenzene degradation in Fenton-like systems using Cu(II) as catalyst. Comparison between Cu(II)- and Fe(III)-based systems. *Chemical Engineering Journal* **228**, 1148–1157. https://doi.org/10.1016/j.cej.2013.05.002.

Niu, P., Zhang, L., Liu, G. & Cheng, H. M. 2012 Graphene-like carbon nitride nanosheets for improved photocatalytic activities. *Advanced Functional Materials* **22**, 4763–4770. https://doi.org/10.1002/adfm.201200922.

Pisanu, A., Speltini, A., Vigani, B., Ferrari, F., Mannini, M., Calisi, N., Cortigiani, B., Caneschi, A., Quadrelli, P., Profumo, A. & Malavasi, L. 2018 Enhanced hydrogen photogeneration by bulk g-C_3N_4 through a simple and efficient oxidation route. *Dalton Transactions* **47** (19), 6772–6778. https://doi.org/10.1039/C8DT00276B.

Sudhaik, A., Raizada, P., Shandilya, P., Jeong, D. Y., Lim, J. H. & Singh, P. 2018 Review on fabrication of graphitic carbon nitride based efficient nanocomposites for photodegradation of aqueous phase organic pollutants. *Journal of Industrial and Engineering Chemistry* **67**, 28–51. https://doi.org/10.1016/j.jiec.2018.07.007.

Wang, X. & Nan, Z. 2020 Highly efficient Fenton-like catalyst Fe-g-C_3N_4 porous nanosheets formation and catalytic mechanism. *Separation and Purification Technology* **233**, 116023. doi:10.1016/j.seppur.2019.116023.

Xu, J., Zhang, L., Shi, R. & Zhu, Y. 2013 Chemical exfoliation of graphitic carbon nitride for efficient heterogeneous photocatalysis. *Journal of Materials Chemistry A* **1**, 14766–14772. https://doi.org/10.1039/C3TA13188B.

Zhao, H., Yu, H., Quan, X., Chen, S., Zhao, H. & Wang, H. 2014 Atomic single layer graphitic-C_3N_4: fabrication and its high photocatalytic performance under visible light irradiation. *RSC Advances* **4**, 624–628. https://doi.org/10.1039/C3RA45776A.

Zhu, Y., Zhu, R., Xi, Y., Zhu, J., Zhu, G. & He, H. 2019 Strategies for enhancing the heterogeneous Fenton catalytic reactivity: a review. *Applied Catalysis B: Environmental* **255**, 117739. https://doi.org/10.1016/j.apcatb.2019.05.041.

Zhu, R. L., Zhu, Y. P., Xian, H. Y., Yan, L. X., Fu, H. Y., Zhu, G. Q., Xi, Y. F., Zhu, J. X. & He, H. P. 2020a CNTs/ferrihydrite as a highly efficient heterogeneous Fenton catalyst for the degradation of bisphenol A: the important role of CNTs in accelerating Fe(III)/Fe(II) cycling. *Applied Catalysis B: Environmental* **270**, 118891. https://doi.org/10.1016/j.apcatb.2020.118891.

Zhu, G. X., Lu, T. L., Han, L. & Zhan, Y. Z. 2020b Graphitic carbon nitride (g-C_3N_4) as an efficient metal-free Fenton-like catalyst for degrading organic pollutants: the overlooked non-photocatalytic activity. *Water Science and Technology* **81** (3), 518–528. https://doi.org/10.2166/wst.2020.129.

First received 3 February 2021; accepted in revised form 14 July 2021. Available online 22 July 2021